



HAL
open science

Determination of the affinity of biomimetic peptides for uranium through the simultaneous coupling of HILIC to ESI-MS and ICP-MS

Lana Abou Zeid, Albert Pell, Marta Garcia Cortes, H el ene Isnard, Pascale Delangle, Carole Bresson

► To cite this version:

Lana Abou Zeid, Albert Pell, Marta Garcia Cortes, H el ene Isnard, Pascale Delangle, et al.. Determination of the affinity of biomimetic peptides for uranium through the simultaneous coupling of HILIC to ESI-MS and ICP-MS. *Analytica Chimica Acta*, 2023, 1242, pp.340773. 10.1016/j.aca.2022.340773 . cea-03940809

HAL Id: cea-03940809

<https://cea.hal.science/cea-03940809>

Submitted on 16 Jan 2023

HAL is a multi-disciplinary open access archive for the deposit and dissemination of scientific research documents, whether they are published or not. The documents may come from teaching and research institutions in France or abroad, or from public or private research centers.

L'archive ouverte pluridisciplinaire **HAL**, est destin ee au d ep ot et  a la diffusion de documents scientifiques de niveau recherche, publi es ou non,  emanant des  tablissements d'enseignement et de recherche fran ais ou  trangers, des laboratoires publics ou priv es.

Determination of the affinity of biomimetic peptides for uranium through the simultaneous coupling of HILIC to ESI-MS and ICP-MS

Lana ABOU-ZEID^{a, c, #}, Albert PELL^a, Marta GARCIA CORTES^a, H el ene ISNARD^a,

Pascale DELANGLE^b and Carole BRESSON^{a*}

^a Universit e Paris-Saclay, CEA, Service d'Etudes Analytiques et de R eactivit e des Surfaces F-91191, Gif-sur-Yvette, France

^b Univ. Grenoble Alpes, CEA, CNRS, GRE-INP, IRIG, SyMMES, 38 000 Grenoble, France

^c Sorbonne Universit e, UPMC, F-75005 Paris, France

Current address: Department of Analytical Chemistry, Ghent University, Krijgslaan 281-S12, 9000 Ghent, Belgium

* CORRESPONDING AUTHOR: Carole BRESSON

Email address: carole.bresson@cea.fr

KEYWORDS: Uranyl, multi-phosphorylated peptides, simultaneous coupling, HILIC, ESI-MS, ICP-MS, affinity scale

1 Abstract

2 Several proteins have been identified in the past decades as targets of uranyl (UO_2^{2+}) *in vivo*. However,
3 the molecular interactions responsible for this affinity are still poorly known which requires the
4 identification of the UO_2^{2+} coordination sites in these proteins. Biomimetic peptides are efficient
5 chemical tools to characterize these sites. In this work, we developed a dedicated analytical method to
6 determine the affinity of biomimetic, synthetic, multi-phosphorylated peptides for UO_2^{2+} and evaluate
7 the effect of several structural parameters of these peptides on this affinity at physiological pH. The
8 analytical strategy was based on the implementation of the simultaneous coupling of hydrophilic
9 interaction chromatography (HILIC) with electrospray ionization mass spectrometry (ESI-MS) and
10 inductively coupled plasma mass spectrometry (ICP-MS). An essential step had been devoted to the
11 definition of the best separation conditions of UO_2^{2+} complexes formed with di-phosphorylated peptide
12 isomers and also with peptides of different structure and degrees of phosphorylation. We performed the
13 first separations of several sets of UO_2^{2+} complexes by HILIC ever reported in the literature. A dedicated
14 method had then been developed for identifying the separated peptide complexes online by ESI-MS and
15 simultaneously quantifying them by ICP-MS, based on uranium quantification using external
16 calibration. Thus, the affinity of the peptides for UO_2^{2+} was determined and made it possible to
17 demonstrate that (i) the increasing number of phosphorylated residues (pSer) promotes the affinity of
18 the peptides for UO_2^{2+} , (ii) the position of the pSer in the peptide backbone has very low impact on this
19 affinity (iii) and finally the cyclic structure of the peptide favors the UO_2^{2+} complexation in comparison
20 with the linear structure. These results are in agreement with those previously obtained by spectroscopic
21 techniques, which allowed to validate the method. Through this approach, we obtained essential
22 information to better understand the mechanisms of toxicity of UO_2^{2+} at the molecular level and to
23 further develop selective decorporating agents by chelation.

26 Introduction

27 The occurrence of uranium (U) in the environment is due to natural and anthropogenic sources [1].
28 Being part of the actinide family, U has no biological function and exhibits chemical and radiological
29 toxicity, depending on its isotopic composition. Natural U (U_{nat}) displays mainly chemical toxicity
30 driven by the interactions of the uranyl cation (UO_2^{2+}) with target biomolecules *in vivo* [2]. However,
31 the mechanisms of toxicity of UO_2^{2+} at the cellular and molecular level are still poorly understood. The
32 full identification of biomolecules binding specifically UO_2^{2+} *in vivo* and *in vitro* and the characterization
33 of their interactions are essential to better describe these mechanisms and to further develop selective
34 decorporating agents. Although few target proteins of UO_2^{2+} have been identified *in vivo* [3,4], the
35 coordination sites responsible for their strong affinity for UO_2^{2+} are still not known. In this context
36 biomimetic approaches, based on the synthesis of model peptides designed specifically to mimic the
37 coordination sites of UO_2^{2+} in proteins, are very useful to determine the key parameters governing this
38 affinity [5]. Recently, multi-phosphorylated cyclopeptides have been synthesized as models of UO_2^{2+}
39 coordination sites in osteopontin (OPN) (Fig.1), a hyperphosphorylated target protein of UO_2^{2+} [4,6].
40 Such biomimetic peptides need to be validated to be representative of the suggested UO_2^{2+} coordination
41 sites. In this purpose, studies have been devoted to the characterization of UO_2^{2+} interactions with these
42 peptides and the determination of the associated stability constants using spectroscopic techniques such
43 as fluorescence spectroscopy, Extended X-ray absorption fine structure (EXAFS), circular dichroism
44 (CD) and also electrospray ionization mass spectrometry (ESI-MS) [6–10]. Through these studies, the
45 affinity of these peptides for UO_2^{2+} was shown to increase with the number of phosphoserine residues
46 (pSer) in their scaffold, to reach the highest value for tetra-phosphorylated peptide (pS1368), being close
47 to the affinity constant of $UO_2(\text{OPN})$ [6].
48 The aim of this work was to develop a dedicated analytical method to determine in a single step an
49 affinity scale of multi-phosphorylated biomimetic peptides for UO_2^{2+} . The strategy was based on the
50 setting up of the simultaneous coupling of hydrophilic interaction liquid chromatography (HILIC) to
51 electrospray ionization mass spectrometry (ESI-MS) and inductively coupled plasma mass spectrometry
52 (ICP-MS) [11,12]. The $UO_2(\text{peptide})$ complexes could then be separated, online identified by ESI-MS

53 and quantified by ICP-MS in a simultaneous manner. Hence, the quantitative distribution of UO_2^{2+}
54 within the different complexes could be determined in one single step, leading to the further
55 determination of an affinity scale. Through this approach, complementary data to those obtained by
56 spectroscopic techniques could be acquired in combination with the reduction of analysis time and
57 sample consumption, which is a major advantage when only small amount of the peptides can be
58 synthesized. A major challenge was to achieve the chromatographic separation of the UO_2^{2+} complexes
59 while preserving the integrity of their structure, knowing that their labile character and their electrostatic
60 interactions can lead to their dissociation during the separation processes [13]. The separation mode of
61 HILIC seemed promising to meet this challenge since it is dedicated to the separation of polar,
62 hydrophilic, neutral or charged compounds and is described as being suitable for the separation of metal
63 complexes, even the labile ones [14]. To our knowledge, the separation of UO_2^{2+} complexes by HILIC
64 has never been reported in the literature.

65 The first part of this work was devoted to the definition of HILIC separation conditions of several model
66 systems containing (i) UO_2^{2+} with di- and tetra-phosphorylated peptides, pS16 and pS1368, in order to
67 determine the effect of the number of pSer residues on UO_2^{2+} affinity (ii) UO_2^{2+} and di-phosphorylated
68 peptide isomers, pS16 and pS18, in order to evaluate the impact of the position of pSer residues on
69 UO_2^{2+} affinity, (iii) UO_2^{2+} in presence of cyclic pS1368 and linear linS1368 tetra-phosphorylated
70 peptides, in order to evaluate the impact of the peptide structure on its affinity for UO_2^{2+} . Then a
71 quantification method of UO_2^{2+} based on external calibration was developed to determine online the
72 distribution of UO_2^{2+} within the separated complexes. Such a dedicated method allowed to measure in
73 a single step the affinity of biomimetic peptides towards UO_2^{2+} when they are in competing
74 complexation reaction and to determine the effect of the structural parameters of the peptides on their
75 affinity.

1. Experimental part

1.1. Chemicals

Acetonitrile (ACN, CH₃CN, LC-MS grade) and ammonia NH₃ (20-22%) were purchased from VWR prolabo (Briare le canal, France). Ammonium acetate (NH₄CH₃CO₂) and toluene (C₆H₅CH₃, purity > 99.7 %) were supplied by Sigma Aldrich (Saint Quentin Fallavier, France). Ultrapure water (18.2 MΩ cm at 25°C) was obtained from Milli-Q purification system (Merck millipore, Guyancourt, France). Uranium (U) and bismuth (Bi) standard solutions (1000 µg mL⁻¹) in HNO₃ 2% w/w, were provided by the SPEX Certiprep Group (Longjumeau, France). L-Tryptophan (Trp) (99% purity) was purchased from Acros Organics. Nitric acid solutions (HNO₃ 2%) were prepared by diluting in ultrapure water, HNO₃ 65% (Merck, France) which was distilled with evapoclean from Analab (France).

1.2. Preparation of stock solutions and samples

1.2.1. Uranium and peptide stock solutions

The uranium stock solution was prepared by diluting in ultrapure water an in-house U_{nat} solution [15] prepared in 0.5 mol L⁻¹ ultrapure HNO₃ (SCP Science), to achieve a U_{nat} concentration of 10,000 µg mL⁻¹ (5 x 10⁻² mol L⁻¹). The U_{nat} concentration of the stock solution was determined by ICP-MS based on external calibration using U_{nat} standard solutions in HNO₃ 2% and was 9,447.2 µg mL⁻¹ (3.97 x 10⁻² mol L⁻¹).

Di-phosphorylated peptide isomers pS16 and pS18 were synthesized, characterized and supplied by the CIBEST team at SyMMES (Univ. Grenoble Alpes, CEA, CNRS, IRIG, 38 000 Grenoble - France) following the procedures described elsewhere [8]. Linear and cyclic tetra-phosphorylated peptides pS1368 and linS1368, were supplied by Cambridge peptides (Cambridge, UK) following the procedure developed by the CIBEST team [6]. The peptide stock solutions were prepared by dissolving the adequate amount of the targeted peptide powder in 20 mmol L⁻¹ NH₄CH₃CO₂ (pH ~ 7.4) to reach a concentration between 2 and 4 mmol L⁻¹. The concentration of the peptides was determined by external calibration, using HILIC coupled to UV/VIS in series with ESI-MS, by quantifying the Tryptophan (Trp) contained in the sequence of all peptides (UV absorption at λ = 280 nm). Trp standard solutions were obtained by diluting a Trp solution prepared at 10⁻² mol L⁻¹ in 20 mmol L⁻¹ NH₄CH₃CO₂, in 70/30

103 ACN/H₂O containing 20 mmol L⁻¹ NH₄CH₃CO₂ to reach concentrations that ranged between 5 x10⁻⁶
104 mol L⁻¹ and 2 x 10⁻⁴ mol L⁻¹.

105 *1.2.2. Preparation of the samples*

106 In a first step, UO₂(peptide) contact solutions were prepared by adding a very small volume (around 1.5
107 μL) of U_{nat} stock solution in 125-250 μL of peptide stock solution, to obtain UO₂²⁺ concentration ranging
108 between 2 and 5 x 10⁻⁴ mol L⁻¹ and the desired UO₂²⁺/peptide ratio. The pH was adjusted to 7.4 using
109 ammonia (20-22%). All solutions were systematically prepared the day before the analysis. Finally, the
110 working samples were freshly prepared before analysis by diluting the UO₂(peptide) contact solutions
111 by a factor of 2 or 5 in the adequate mobile phase, to reach a final UO₂²⁺ concentration of 10⁻⁴ mol L⁻¹,
112 which was quantified by ICP-MS as described in section 1.4.1. The concentration of the peptides in the
113 contact solution was determined by weight while taking into account the concentration of the peptide
114 stock solution.

115 **1.3. Instrumentation**

116 *1.3.1. Hydrophilic interaction liquid chromatography*

117 An ultimate 3000 UHPLC⁺ Dionex/ThermoFisher scientific (Courtaboeuf, France), made of a degasser,
118 a dual RS pump, an RS autosampler, a column compartment and an RS diode array detector, was used.
119 The separation of the different sets of UO₂(peptide) complexes was carried out using Acquity BEH
120 Amide (100 x 2.1; 1,7 μm, Waters), YMC Triart Diol (100 x 2; 1.9 μm, YMC) and Acquity BEH HILIC
121 (100 x 2.1; 1,7 μm, Waters) columns. The composition of the desired mobile phases was obtained by
122 online mixing in the adequate proportions, solvent A (60/40 ACN/H₂O v/v containing 20 mmol L⁻¹
123 NH₄CH₃CO₂) and solvent B (80/20 ACN/H₂O v/v containing 20 mmol L⁻¹ NH₄CH₃CO₂).

124 For the quantification of pS16, pS18 and pS1368 stock solutions, an YMC Triart diol (100 x 2 mm; 1,9
125 μm) column was used with a mobile phase composed of 70/30 ACN/H₂O v/v and 20 mmol L⁻¹
126 NH₄CH₃CO₂. For the quantification of linS1368, an Acquity BEH HILIC (100 x 2,1; 1,7μm) column
127 was used and the mobile phase was made of 68/32 ACN/H₂O v/v and 20 mmol L⁻¹ NH₄CH₃CO₂. In all
128 the cases, the separation was run in isocratic mode at a flow rate of 300 μL min⁻¹ and the injection
129 volume was 3 μL.

130 The retention factor k of the analytes were calculated following the equation (1):

$$131 \quad k = \frac{(t_R - t_0)}{t_0} \text{ (Equation 1)}$$

132 Where t_R is the retention time (min) of the analyte, determined by HILIC-ESI-MS, t_0 is the void time of
133 unretained marker, toluene (10^{-4} mol L $^{-1}$, $V_{inj} = 1$ μ L), determined by HILIC-UV/VIS at $\lambda = 254$ nm.

134 The selectivity and resolution factors of the separations, α and R_s respectively, were calculated based on
135 the equations 2 and 3:

$$136 \quad \alpha = \frac{k_2}{k_1} \text{ (Equation 2)}$$

$$137 \quad R_s = 1.18 \times \frac{t_{R2} - t_{R1}}{W_{0.5h1} + W_{0.5h2}} \text{ (Equation 3)}$$

138 With analyte 2 more retained than analyte 1. $W_{0.5}$ corresponds to full width half-maximum of each peak.

139 *1.3.2. Mass spectrometers*

140 The ESI mass spectrometer was a triple quadrupole TSQ Quantum UltraTM (Thermo Fisher scientific,
141 San Diego CA, USA) equipped with an H-ESI II ionization probe. All mass spectra were recorded in
142 negative ionization mode with the following parameters: spray voltage -3.5 kV, temperature of the probe
143 120°C and temperature of the capillary transfer 360°C. In all cases and in agreement with previous
144 studies [6,8], double charged $[\text{UO}_2(\text{peptide})]^{2-}$ complexes with 1:1 stoichiometry were observed. For
145 the sake of clarity, the UO_2^{2+} complexes were denoted along the manuscript $\text{UO}_2(\text{peptide})$, by omitting
146 the charge. Mass spectra were acquired in full scan mode (m/z 400-1500) and in single ion monitoring
147 (SIM) mode, by selecting the m/z ratio associated to the targeted free peptides and $\text{UO}_2(\text{peptide})$
148 complexes (spectral width: ± 0.5 m/z).

149 The ICP-MS instrument was a single quadrupole XSeriesII (Thermo Fisher Scientific). The sample
150 introduction system consisted of a perfluoroalkoxy PFA-ST nebulizer operating at 200 μ L min $^{-1}$
151 followed by a quartz cyclonic spray chamber thermostated at 3 °C (PC3 system, ESI). The simultaneous
152 coupling of HILIC to ESI-MS and ICP-MS was performed according to the setting up described in our
153 previous work [11] and presented in Fig.2. In order to prevent any carbon deposition due to the use of
154 organic solvents, additional 8 mL min $^{-1}$ oxygen flow rate was introduced in the plasma, through an
155 “additional gas port” located in the spray chamber [16,17]. A platinum skimmer, a sampler cone and a

156 1 mm inner diameter injector were additionally used for this purpose. The parameters were checked
157 daily using a 25 ng mL⁻¹ U_{nat} standard solution introduced in the ICP-MS at 6.7 μL min⁻¹ along with a
158 10 ng mL⁻¹ Bi in HNO₃ 2% at 140 μL min⁻¹ (Fig.2). The chromatograms were recorded based on the
159 signal of ²³⁸U and ²⁰⁹Bi with an integration time of 90 ms for each isotope.

160 **1.4.Online quantification of the UO₂(peptide) complexes**

161 Samples were analyzed using the simultaneous coupling of HILIC to ESI-MS and ICP-MS. The
162 separated UO₂(peptide) complexes were online identified by ESI-MS and simultaneously quantified by
163 ICP-MS. For this purpose, external calibration was selected as quantification method for the
164 determination of total UO₂²⁺ concentration in the samples, denoted [UO₂²⁺]_{total}, since the uncertainty
165 range (5-15%) provided by this method is adequate for our study.

166 *1.4.1. Determination of the total UO₂²⁺ concentration in the working samples*

167 Calibration was performed by introducing U_{nat} standard solutions into the ICP-MS under flow injection
168 analysis mode (FIA), employing the same mobile phase composition and flow rate as used when
169 coupling to the separation. In non-complexing medium, hydrolysis dominates the speciation of UO₂²⁺,
170 potentially leading to its precipitation depending on its concentration [18]. Therefore, the tetra-
171 phosphorylated peptide pS1368 was added to the U_{nat} standard solutions in an equimolar ratio to prevent
172 this phenomenon, but also to yield specific standard solutions of UO₂(peptide) complexes. Five levels
173 of calibration were considered with U_{nat} concentration ranging from 8 to 40 μg mL⁻¹. The calibration
174 curve was established daily by plotting the mean value of the peak areas as a function of U_{nat}
175 concentrations; each standard being injected in triplicate. The repeatability of the measurements,
176 determined from the RSD of the peak areas for each concentration, was between 1% and 4% (< 15%).

177 *1.4.2. Quantification of UO₂²⁺ in the separated UO₂(peptide) complexes*

178 This step was performed by integrating the total area of the chromatographic peak of each UO₂(peptide)
179 complex and by further determining the corresponding concentration using the calibration curve. During
180 the separation, adsorption of free or weakly complexed UO₂²⁺, on the stationary phase can occur. To
181 recover UO₂²⁺ adsorbed on the column, successive injections of the tetra-phosphorylated peptide pS1368
182 were carried out after each chromatographic run until the background of ²³⁸U signal was less than 10³

183 cps. The concentration of this fraction of UO_2^{2+} , denoted $[\text{UO}_2^{2+}]_{\text{free}}$, was then determined based on
184 external calibration, by summing the area of the peaks resulting from the injections of pS1368. A
185 cleaning process was further carried out to eliminate any adsorbed peptide residues, using 5/95
186 ACN/ H_2O v/v containing 20 mmol L^{-1} CH_3COOH , followed by the column regeneration with the
187 working mobile phase working.
188 The quantitative distribution of UO_2^{2+} among the eluted species, expressed in percent (%), was
189 determined according to the Equation 4.

$$190 \quad \% \text{UO}_2^{2+}_X = \frac{[\text{UO}_2^{2+}]_X}{[\text{UO}_2^{2+}]_{\text{total}}} \text{ (Equation 4)}$$

191 With X being free UO_2^{2+} or $\text{UO}_2(\text{peptide})$ complexes.

192 The mass balance was expressed as the ratio of the sum of the concentrations of UO_2^{2+} in its free and
193 complexed forms, to the total concentration of UO_2^{2+} in the sample, according to Equation 5.

$$194 \quad \text{Mass balance (\%)} = \frac{\sum [\text{UO}_2^{2+}]_{\text{UO}_2(\text{peptide}1)} + [\text{UO}_2^{2+}]_{\text{UO}_2(\text{peptide}2)} + [\text{UO}_2^{2+}]_{\text{Free}}}{[\text{UO}_2^{2+}]_{\text{total}}} \text{ (Equation 5)}$$

195 During the HILIC-ICP-MS coupling and the FIA mode, the stability of the ^{238}U signal was monitored
196 using bismuth (^{209}Bi) as internal standard, added at 10 ng mL^{-1} in the nitric acid makeup solution (Fig.).
197 The stability of the ^{209}Bi signal during an acquisition cycle was checked by calculating the relative
198 standard deviation RSD (%) of measurements acquired continuously. The RSD was 1.9%, which reflects
199 good stability of the signal during an acquisition cycle (< 15%). The stability of the ICP-MS response
200 was also daily checked by calculating the standard deviation of the averaged ^{209}Bi measurements for all
201 acquisitions cycles. As for example, for a maximum of 11 acquisition cycles, an RSD between 1 and
202 5.9% was obtained, which is acceptable for our applications.

203

204 **2. Results and discussion**

205 **2.1. Definition of the HILIC conditions for separating UO₂(peptide) complexes**

206 The achievement of the HILIC separation of the UO₂(peptide) complexes is a crucial step to be able to
207 develop our method. Due to the particularity of UO₂²⁺ complexes, few chromatographic techniques are
208 suitable to perform such challenging separations [13]. The ones encountered in the literature are mainly
209 size exclusion chromatography (SEC) [3,19–23] and immobilized metal affinity chromatography
210 (IMAC) [24], to investigate the interactions of UO₂²⁺ with proteins. Furthermore, the limitation of these
211 separation techniques lies in their low separation resolution and in some cases their incompatibility to
212 ESI-MS coupling. The preservation of UO₂²⁺ complexes during elution is of great concern since
213 dissociation is often observed for such labile species during the chromatographic process. Even though
214 the UO₂(peptide) complexes are known to be fully formed in the samples as indicated by their stability
215 constants measured at pH 7.4 [6,10], they may fully or partially dissociate on the column. One way to
216 limit this dissociation is to use an excess of the peptides in the samples. However, full dissociation was
217 observed for complexes containing cyclic peptides with no or only one pSer in their sequence, whatever
218 the column and the UO₂²⁺:peptide proportion (data not shown). By contrast, UO₂²⁺ complexes with
219 multi-phosphorylated peptides and having stability constants higher or equal to 10¹⁰, could be detected
220 using an excess of di- and tetra-phosphorylated peptides, from 2 to 10 equivalents. It must be mentioned
221 that several UO₂²⁺:peptide proportions were tested, but only the chromatograms obtained with the
222 proportions that allowed to detect all the separated complexes, at least by ICP-MS, are presented in this
223 part.

224 In our previous work, the Acquity BEH amide column with a mobile phase made of 70/30 ACN/H₂O
225 v/v and 20 mmol L⁻¹ NH₄CH₃CO₂ allowed a successful separation of the free multi-phosphorylated
226 peptides [25]. Therefore, we first evaluated these conditions to separate the UO₂²⁺ complexes containing
227 these peptides, but successful results were obtained only for the complexes formed with the ps16 and
228 ps18 isomers (Fig.1). As shown in Fig.3-a, UO₂(pS16) and UO₂(pS18) complexes were separated with
229 a good selectivity ($\alpha=1.3$) and baseline resolution ($R_s= 2.2$). The availability of the pSer group in
230 different positions in the peptide scaffold (Fig.1) could explain the achievement of the separation

231 through differential interactions of the pSer with the amide function of the stationary phase, as
232 previously observed for the free peptides [25].

233 As stated above, these chromatographic conditions did not allow the separation of the $\text{UO}_2(\text{pS16})/$
234 $\text{UO}_2(\text{pS1368})$ and $\text{UO}_2(\text{pS1368})/ \text{UO}_2(\text{linS1368})$ sets of complexes, even by increasing the acetonitrile
235 content of the mobile phase while keeping the salt concentration constant. A less polar stationary phase,
236 grafted by diol functional group (YMC Triart Diol) led to the separation of $\text{UO}_2(\text{pS16})$ and $\text{UO}_2(\text{pS1368})$
237 with an improved selectivity ($\alpha = 2.3$) and resolution ($R_s = 3.9$), using 72% of ACN in the mobile phase
238 (Fig.3-b). As seen in (Fig.3-b), the $\text{UO}_2(\text{pS16})$ complex could not be observed by ESI-MS despite the
239 high excess of pS16 added to pS1368 and UO_2^{2+} . In the chromatogram recorded by ICP-MS, we could
240 observe a peak of low intensity eluting at the same retention time as free pS16, which may be reasonably
241 assigned to $\text{UO}_2(\text{pS16})$. The peak eluting at 4 min was attributed to $\text{UO}_2(\text{pS1368})$, thanks to its
242 identification by ESI-MS. Furthermore, free pS1368 was not detected by ESI-MS, allowing to suggest
243 that this peptide, which exhibits a high affinity for UO_2^{2+} , is fully coordinated.

244 Acquity BEH HILIC hybrid silica column was selected to separate $\text{UO}_2(\text{pS1368})$ and $\text{UO}_2(\text{linS1368})$
245 containing tetra-phosphorylated peptides having the same peptide sequence but different cyclic/linear
246 structure. A mobile phase composed of 68/32 ACN/ H_2O v/v and 20 mmol L^{-1} $\text{NH}_4\text{CH}_3\text{CO}_2$ yielded the
247 best separation of the two complexes with good selectivity ($\alpha=8.1$) and resolution ($R_s=5.6$) (Fig.3-c).
248 The UO_2^{2+} complex formed with the cyclic peptide eluted earlier than the complex containing the linear
249 one. This allows to suggest that the accessibility of the polar groups of the stationary phase to interact
250 with the complexes is linked to the structuration of the peptide upon its complexation to UO_2^{2+} . To our
251 knowledge, the use of hybrid silica column has never been described in the literature to separate metal
252 complexes. Only one study reports the use of a bare silica column to separate gadolinium-based contrast
253 agents [26], while most of the separations of transition metal complexes such as Fe, Cu and Ni, were
254 carried out with stationary phases grafted by zwitterionic, diol and amide functions [14,27]. In our study,
255 dedicated HILIC conditions were set up to successfully separate a set of $\text{UO}_2(\text{peptide})$ complexes with
256 good selectivity and baseline resolution. These results highlight the potential of HILIC to separate UO_2^{2+}
257 complexes, known to be challenging. Thus, we reported the first separations of UO_2^{2+} complexes ever
258 described in the literature, using HILIC.

2.2 Evaluation of the effect of the structure of the peptides on UO_2^{2+} affinity

2.2.1. Effect of the number of phosphorylated residues in the peptide backbone

When designing biomimetic peptides, the selection of the amino acid to build the peptide backbone is of prime importance since the functional complexing groups of these amino acids will be involved in the UO_2^{2+} coordination. Phosphorylated amino acids, mainly pSer are of major concern, knowing that UO_2^{2+} exhibits high affinity for phosphate groups [28]. Furthermore, some of UO_2^{2+} target proteins such as OPN, are highly phosphorylated and are suspected to interact with UO_2^{2+} through their pSer sites [6,29]. Therefore, the effect of phosphorylation on UO_2^{2+} affinity has gained a lot of interest and was studied by using a peptide representative of site 1 of calmodulin [30,31] and phosphorylated model peptides of a specific sequence of β -casein [32]. The phosphorylation of these model peptides induced an increase of their affinity towards UO_2^{2+} in comparison to their non-phosphorylated counterparts.

In our work, the effect of phosphorylation on UO_2^{2+} affinity was evaluated in a single step by applying the analytical approach that we developed through the simultaneous coupling of HILIC to ESI-MS and ICP-MS. Several ratios of di- and tetra-phosphorylated peptides pS16 and pS1368 were added to UO_2^{2+} at pH 7.4. Knowing that the conditional stability constant of $\text{UO}_2(\text{pS16})$ is lower than that of $\text{UO}_2(\text{pS1368})$ (Fig.1), a higher excess of pS16 was added to UO_2^{2+} in comparison to pS1368. The quantitative distribution of UO_2^{2+} among the separated peptide complexes was determined through the quantification method described in the experimental part, which allowed to assess the differential affinity of the peptides towards UO_2^{2+} . The total UO_2^{2+} concentration in each sample was firstly measured in duplicate by ICP-MS before the separation and the values are listed in Table 1, as well as targeted and experimental $x\text{UO}_2^{2+}:y\text{pS1368}:z\text{pS16}$ proportions.

Table 1: Total concentration of UO_2^{2+} in each sample $[\text{UO}_2^{2+}]_{\text{total}}$ measured in duplicate, relative deviation* of the values, experimental concentration of pS1368 and pS16 in the samples and experimental $x\text{UO}_2^{2+}:y\text{pS1368}:z\text{pS16}$ proportions. For simplification, the samples containing different x:y:z proportions were assigned by a letter (A-E).

Targeted $x\text{UO}_2^{2+}:y\text{pS1368}:z\text{pS16}$	$[\text{UO}_2^{2+}]_{\text{total}}$ $\mu\text{g mL}^{-1}$ (mol L^{-1})		Relative deviation* (%)	$[\text{pS1368}]$ mol L^{-1}	$[\text{pS16}]$ mol L^{-1}	Experimental $x\text{UO}_2^{2+}:y\text{pS1368}$ $:z\text{pS16}$ (sample N)
	Value 1	Value 2				
2:0:20	20.5 (8.6×10^{-5})	20.3 (8.5×10^{-5})	1.2	0	9.2×10^{-4}	2:0:21.2 (A)
2:0.5:20	20.8 (8.7×10^{-5})	20.9 (8.8×10^{-5})	0.7	2.3×10^{-5}	9.1×10^{-4}	2:0.5:20.9 (B)
2:2:2	30.5 (1.3×10^{-4})	31.4 (1.3×10^{-4})	2.9	1.2×10^{-4}	1.2×10^{-4}	2:1.9:1.9 (C)
2:3:1	39.8 (1.7×10^{-4})	39.7 (1.7×10^{-4})	0.3	1.7×10^{-4}	6.0×10^{-5}	2:2.1:0.7 (D)

2:4:0	33.9 (1.4 x10 ⁻⁴)	35.5 (1.5 x10 ⁻⁴)	4.6	4.6 x10 ⁻⁴	0.0	2:6.4:0 (E)
--------------	-------------------------------	-------------------------------	-----	-----------------------	-----	-------------

*Relative deviation (value1-value 2)/(value 1)

284 As can be seen in Table 1, a relative deviation ranging between 0.3 and 4.6 % shows good repeatability
 285 of the measurements.

286 The chromatograms simultaneously recorded by ESI-MS and ICP-MS, using the YMC Triart Diol
 287 column to separate the complexes, are presented in Fig.4. The peak of free tetra-phosphorylated peptide
 288 pS1368 was observed by ESI-MS only when it was in excess relatively to UO₂²⁺, whereas the one of
 289 pS16 was detected for all proportions. The peak corresponding to UO₂(pS1368) was detected by ESI-
 290 MS and ICP-MS for all proportions whilst the one of UO₂(pS16) was observed exclusively by ICP-MS
 291 and only when pS16 was in large excess compared to UO₂²⁺ and pS1368, that is for samples A and B.
 292 This indicates that pS1368 seems to fully complex UO₂²⁺ when they are in equimolar proportions or
 293 less, while pS16 is weakly complexed even when it is present in large excess with respect to UO₂²⁺. The
 294 quantitative distribution of total UO₂²⁺ among the di- and tetra-phosphorylated peptide complexes and
 295 the mass balance, expressed in percent (%) could be calculated using Equation 4 and 5, respectively and
 296 are presented in the diagram of Fig.5. In the presence of three equivalents of pS1368 (Sample E), 93%
 297 of total UO₂²⁺ was involved in UO₂(pS1368) and 5% was under free form. When the proportion of
 298 pS1368 decreased compared to that of pS16, only the fraction of free UO₂²⁺ increased to reach 42% for
 299 equimolar conditions 2UO₂²⁺:2pS1368:2pS16 (sample C), while 56% of total UO₂²⁺ remained involved
 300 in UO₂(pS1368). Even when pS16 was in large excess compared to pS1368 and UO₂²⁺ (Sample B), up
 301 to 91% of total UO₂²⁺ was under free form and the remaining fraction was involved in UO₂(pS1368).
 302 Since UO₂(pS16) could not be quantified, its fraction was estimated to be 0.2% by calculating the ratio
 303 of the peak areas of this complex to that of total UO₂²⁺.

304 Thus, it can be concluded that the addition of three equivalents of pS1368 (Sample E) to UO₂²⁺ led to
 305 the complexation of 93% of the latter, while 10 equivalents of pS16 (Sample A) were not enough to
 306 complex less than 1% of UO₂²⁺. When these two peptides were present in equimolar proportion with
 307 respect to UO₂²⁺, half of the total UO₂²⁺ was complexed by pS1368 while the remaining half was under
 308 free form. This results confirms that the tetra-phosphorylated peptide exhibits a higher affinity for UO₂²⁺

309 compared to the di-phosphorylated one, in agreement with the values of the conditional stability
310 constants previously reported, which allows to validate the method [6].

311 *2.2.2. Effect of the position of phosphorylated residues in the peptide backbone*

312 In addition to the major role played by the number of pSer residues to complex UO_2^{2+} , the coordination
313 ability of these residues might be affected by their position in the peptide backbone and their neighboring
314 amino acids through steric effect [8]. In this part, the impact of the position of pSer residues on UO_2^{2+}
315 affinity was evaluated by adding di-phosphorylated peptide isomers pS16 and pS18 in equimolar
316 proportions to UO_2^{2+} , knowing that these two peptides exhibit the same sequence but the pSer are in
317 different positions in the cyclic peptide scaffold (Fig.1). The formed complexes were separated using
318 the Acquity BEH amide column, and the chromatograms obtained simultaneously by ESI-MS and ICP-
319 MS are presented in Fig.3-a.

320 Since these complexes are identical in terms of structure and charge, the amount of free UO_2^{2+} potentially
321 adsorbed on the column was considered to be also identical. Therefore, the quantitative distribution of
322 UO_2^{2+} among the two isomeric complexes was determined by calculating the ratio of the peak areas
323 $A(^{238}\text{U}_{\text{UO}_2(\text{pS18})})/A(^{238}\text{U}_{\text{UO}_2(\text{pS16})})$ from the chromatograms recorded by ICP-MS, for measurements carried
324 out in triplicate. The average ratio was 1.30 and the RSD was 6.2%, reflecting good repeatability of the
325 measurements. The ratio close to unity shows that UO_2^{2+} did not preferentially coordinate one of the two
326 isomers, allowing to deduce that the position of the pSer group in the peptide backbone has very weak
327 influence on the affinity of these peptides towards UO_2^{2+} . This result is in agreement with the conditional
328 stability constants of the two complexes, being $\log K^{\text{pH}=7.4}(\text{UO}_2(\text{pS18})) = 10.1$ and $\log K^{\text{pH}=7.4}$
329 $(\text{UO}_2(\text{pS16})) = 10.3$ [8].

330 *2.2.3. Effect of the cyclic/linear structure of the peptide backbone*

331 The structure of the biomimetic peptides plays a key role in the coordination of UO_2^{2+} , which is directly
332 related to the degree of flexibility of the peptide backbone [5]. The pre-organized cyclic peptides
333 considered in this work were designed specifically to complex UO_2^{2+} in its equatorial plane (Fig.1).
334 Linear peptides of equivalent sequence are more flexible and must therefore adapt their conformation
335 around UO_2^{2+} for an efficient coordination. The structure of the peptide has therefore a direct effect on

336 its affinity for UO_2^{2+} [7]. In this part, the method developed by HILIC-ESI-MS/ICP-MS was applied to
 337 measure online and in a single step the affinity towards UO_2^{2+} , of tetra-phosphorylated peptides with the
 338 same sequence but cyclic (pS1368) and linear (linS1368) structure. Variable proportions of the pS1368
 339 and linS1368 were added to UO_2^{2+} , in a competitive complexation reaction.
 340 Measured total UO_2^{2+} concentration in each sample before separation, targeted and experimental
 341 $x\text{UO}_2^{2+}:\text{ypS1368}:\text{zlinS1368}$ proportions are summarized in Table 2.

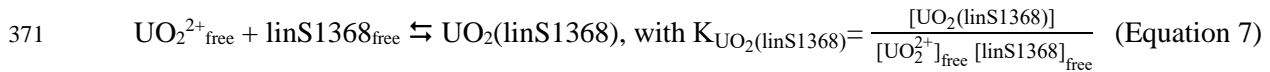
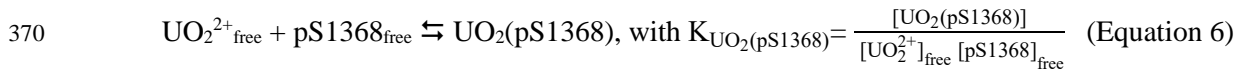
342 Table 2 : Total concentration of UO_2^{2+} in each sample $[\text{UO}_2^{2+}]_{\text{total}}$ measured in duplicate, relative deviation (%)
 343 of the values, experimental concentration of pS1368 and linS1368 in the samples and experimental
 344 $x\text{UO}_2^{2+}:\text{ypS1368}:\text{zlinS1368}$ proportions. For simplification, the samples containing different x:y:z proportions
 345 were assigned by a letter (A-E).

Targeted $x\text{UO}_2^{2+}:\text{ypS1368}:\text{zlinS1368}$	$[\text{UO}_2^{2+}]_{\text{total}}$ $\mu\text{g mL}^{-1}$ (mol L^{-1})		Relative deviation (%)	[pS1368] mol L^{-1}	[linS1368] mol L^{-1}	Experimental $x\text{UO}_2^{2+}:\text{ypS1368}:\text{zlinS1368}$ (sample N)
	Value 1	Value 2				
2:4:0	28.2 (1.2×10^{-4})	28.4 (1.2×10^{-4})	0.7	4.5×10^{-4}	0	2:7.5:0 (A)
2:3:1	27.5 (1.2×10^{-4})	27.6 (1.2×10^{-4})	0.3	1.9×10^{-4}	6.1×10^{-5}	2:3.2:1 (B)
2:2:2	33.9 (1.4×10^{-4})	34.8 (1.5×10^{-4})	2.7	1.4×10^{-4}	1.4×10^{-4}	2:2:1.9 (C)
2:0.5:3.5	24.0 (1.0×10^{-4})	23.9 (1.0×10^{-4})	0.6	3.7×10^{-5}	2.4×10^{-4}	2:0.7:4.6 (D)
2:0:4	28.7 (1.2×10^{-4})	28.1 (1.2×10^{-4})	2.1	0	5.6×10^{-4}	2:0:9 (E)

346 As reported in Table 2, the relative deviation between the values obtained for each replicate was between
 347 0.3 and 2.7%, showing good repeatability of the measurements. The chromatograms simultaneously
 348 recorded by ESI-MS and ICP-MS, using the Aquity BEH HILIC column to separate the complexes, are
 349 shown in Fig.6.

350 As shown in Fig.6, the peak of free pS1368 in the chromatograms recorded by ESI-MS was observed
 351 only when it was in excess relatively to UO_2^{2+} (samples A and B), whilst the one of linS1368 was
 352 detected for all ratios. Furthermore, the peak corresponding to $\text{UO}_2(\text{pS1368})$ was observed by ESI-MS
 353 and ICP-MS for all proportions whilst the one of $\text{UO}_2(\text{linS1368})$ was detected exclusively when
 354 linS1368 was in large excess compared to UO_2^{2+} . All these observations indicate that pS1368 is fully
 355 bound to UO_2^{2+} in equimolar proportion or less, while linS1368 is weakly engaged in the complexation
 356 even when it was added in large excess. The quantitative distribution of total UO_2^{2+} among the different
 357 complexes and the mass balance, expressed in percent (%) could be calculated using Equation 4 and 5,
 358 respectively and are presented in the diagram of Fig.7. When UO_2^{2+} was in the presence of an excess of
 359 pS1368, 97% of total UO_2^{2+} were involved in the complexation while the remaining fraction was under
 360 free form (Sample A). When the proportion of pS1368 decreased in favor of that of its linear equivalent,

361 the fraction of free UO_2^{2+} increased significantly, while the fraction of UO_2^{2+} engaged in $\text{UO}_2(\text{linS1368})$
362 slightly increased (Sample B-D). Finally, excess of linS1368 peptide led to the involvement of only 12%
363 of the total UO_2^{2+} in the corresponding complex, while 77% was in the free form (Sample E).
364 All of these results show that UO_2^{2+} coordinates preferentially the cyclic peptide in comparison with the
365 linear one. The cyclic structure of the peptide confers a higher stability to the UO_2^{2+} complexes than the
366 linear structure, through the more efficient coordination conferred by the preorientation of the four
367 phosphate groups in the equatorial plane of UO_2^{2+} [33]. Owing to our approach, we were able to
368 determine the affinity constant of $\text{UO}_2(\text{linS1368})$. The conditional stability constants of $\text{UO}_2(\text{pS1368})$
369 and $\text{UO}_2(\text{linS1368})$ are expressed according to the equilibria shown in equations 6 and 7.



372 From equations 6 and 7, the logarithmic expression of $\frac{K_{\text{UO}_2(\text{pS1368})}}{K_{\text{UO}_2(\text{linS1368})}}$ is:

373
$$\log \frac{K_{\text{UO}_2(\text{pS1368})}}{K_{\text{UO}_2(\text{linS1368})}} = \log K_{\text{UO}_2(\text{pS1368})} - \log K_{\text{UO}_2(\text{linS1368})} = \log \frac{[\text{linS1368}]_{\text{free}}}{[\text{pS1368}]_{\text{free}}} \text{ (Equation 8)}$$

374
$$\log K^{\text{pH}7.4}(\text{UO}_2(\text{linS1368})) = \log K^{\text{pH}7.4}(\text{UO}_2(\text{pS1368})) - \log \frac{[\text{linS1368}]_{\text{free}}}{[\text{pS1368}]_{\text{free}}} \text{ (Equation 9)}$$

375 The intersection point of the distribution curves of $\text{UO}_2(\text{pS1368})$ and $\text{UO}_2(\text{linS1368})$ fractions (Fig.7)
376 corresponds to an equal percentage of both complexes. allowing to deduce their concentration:
377 $[\text{UO}_2(\text{pS1368})] = [\text{UO}_2(\text{linS1368})] = 7\% \text{ of } [\text{UO}_2^{2+}]_{\text{total}} = 7.11 \pm 0.12 \times 10^{-6} \text{ mol L}^{-1}$, knowing that
378 $[\text{UO}_2^{2+}]_{\text{total}} = 10^{-4} \text{ mol L}^{-1}$.

379 The concentration of linS1368 was deduced from the intersection point Fig.7 and was $3.59 \pm 0.06 \times 10^{-4}$
380 mol L^{-1} , while that of pS1368 was estimated at $2.34 \pm 0.08 \times 10^{-5} \text{ mol L}^{-1}$ by plotting the same curves,
381 but as a function of the pS1368 concentrations. Therefore, a concentration of the linear peptide 15 times
382 higher than that of the cyclic peptide was needed to obtain an equal distribution of UO_2^{2+} between the

383 linear and the cyclic peptide complexes. The total concentrations of the peptides are expressed according
384 to equations 10 and 11:

385
$$[\text{linS1368}]_{\text{Total}} = [\text{UO}_2(\text{linS1368})] + [\text{linS1368}]_{\text{free}} = 3.59 \pm 0.06 \times 10^{-4} \text{ mol L}^{-1} \text{ (Equation 10)}$$

386
$$[\text{pS1368}]_{\text{Total}} = [\text{UO}_2(\text{pS1368})] + [\text{pS1368}]_{\text{free}} = 2.34 \pm 0.08 \times 10^{-5} \text{ (Equation 11)}$$

387 Taking into account the concentrations of the different species calculated above, as well as the value of
388 $\log K^{\text{pH}7.4}(\text{UO}_2(\text{pS1368})) = 11.3$ [6], the equation 8 becomes:

389
$$\log K^{\text{pH}7.4}(\text{UO}_2(\text{linS1368})) = 11.3 - \log(21.64 \pm 1.63) = 9.97 \pm 0.03 \text{ (Equation 12)}$$

390 The constant determined through our methodology allows to deduce that the affinity of the linear tetra-
391 phosphorylated peptide for UO_2^{2+} is more than one order of magnitude lower than its cyclic counterpart
392 at pH 7.4. This result confirms the impact of the peptide structure on the affinity for UO_2^{2+} , that is in
393 agreement with the behavior also observed for proteins. For example, the structure of OPN is not defined
394 and upon complexation with UO_2^{2+} , its secondary structure undergoes modifications to effectively
395 position 4 pSer residues in the UO_2^{2+} equatorial plane [6]. Thus, a structure fitting the coordination of
396 UO_2^{2+} is necessary at the scale of an entire protein as well as at the scale of a small peptide to form
397 UO_2^{2+} complexes of high stability.

398 Conclusion

399 In this work, a dedicated analytical approach was developed to separate UO_2^{2+} complexes formed with
400 multi-phosphorylated biomimetic peptides, to characterize, and quantify them online and in a single
401 step. To reach this aim, we implemented the simultaneous coupling of HILIC to ESI-MS and ICP-MS.
402 Separations of the complexes containing positional isomers, peptides with two and four pSer residues
403 as well as cyclic and linear tetra-phosphorylated peptides of the same sequence, were successfully
404 achieved using columns with amide, diol and hybrid silica stationary phases. We developed the first
405 separations of UO_2^{2+} complexes by HILIC ever described in the literature for complexes with conditional
406 stability constants of 10^{10} or higher at pH 7.4. Owing to the dedicated method that we developed,
407 quantify we were able to determine on line the quantitative distribution of UO_2^{2+} among the separated
408 complexes. Thus, the effect of the structure of the peptides on their affinity towards UO_2^{2+} was
409 determined and we showed that (i) the cyclic tetra-phosphorylated peptide pS1368 has the highest

410 affinity for UO_2^{2+} compared to peptides with a lower degree of phosphorylation, highlighting the high
411 affinity of UO_2^{2+} for phosphate-rich binding sites in proteins. (ii) the pSer position in the peptide
412 sequence had no significant impact on the affinity for UO_2^{2+} , in agreement with the literature results
413 obtained by multiple spectroscopic techniques independently for each sample (iii) the cyclic structure
414 of the tetra-phosphorylated peptide favors the UO_2^{2+} complexation compared to its linear analogue. In
415 addition, we determined the affinity constant of the linear tetra-phosphorylated peptide, being
416 $(\log K^{\text{pH}7.4}(\text{UO}_2(\text{linS1368})) = 9.97 \pm 0.03$.

417 Overall, this work highlights the powerful simultaneous coupling of HILIC to ESIMS and ICPMS to
418 determine in a single step the effect of several structural parameters of biomimetic peptides on their
419 affinity towards UO_2^{2+} when they are in a competing complexation reaction. A quick and reliable
420 determination of stability of the $\text{UO}_2(\text{peptides})$ complexes is of prime importance to access deeper
421 fundamental information on UO_2^{2+} toxicity but also to be able to develop *in vivo* decorporating agents
422 based on chelation. This approach can be extended to the evaluation of the affinity of these biomimetic
423 peptides for other actinides (Pu, Am, Cm...). Moreover, it can be implemented for the screening of the
424 complexation properties of various classes of chelating molecules towards elements of interest in the
425 fields of energy, toxicology and the environment

426

427 **Acknowledgments**

428 The authors would like to acknowledge the Cross-Disciplinary Program on Instrumentation and
429 Detection of CEA, the French Alternative Energies and Atomic Energy Commission and the Cross-
430 cutting basic research Program (RTA Program) of the CEA Energy Division, for their financial support.

431

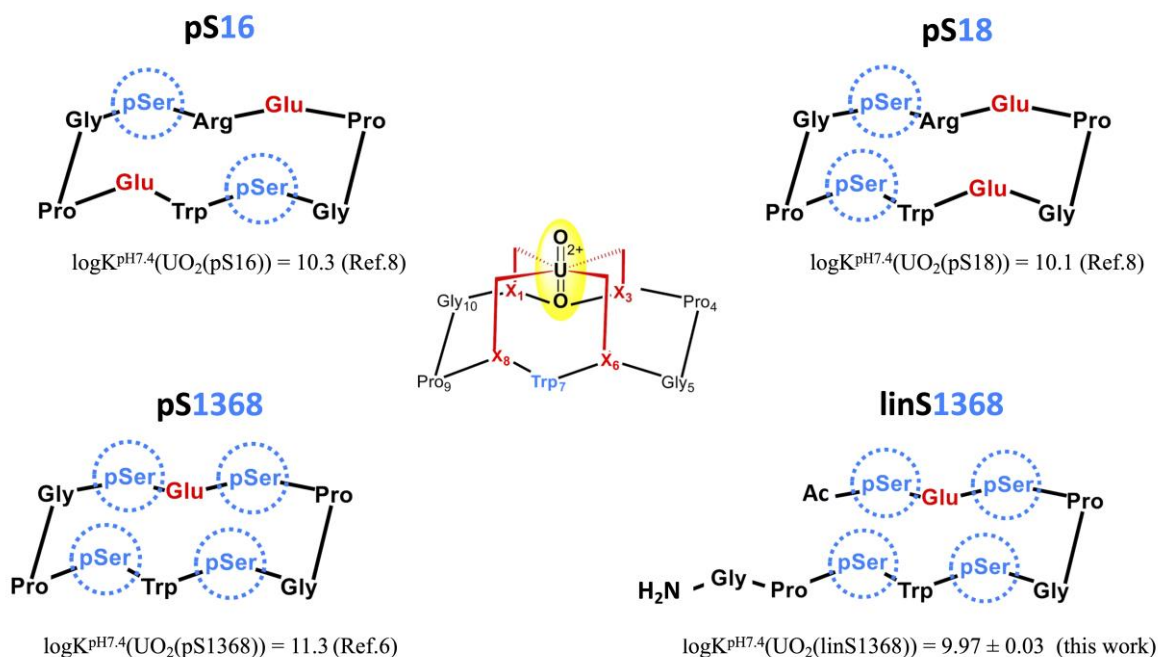
432

433

434

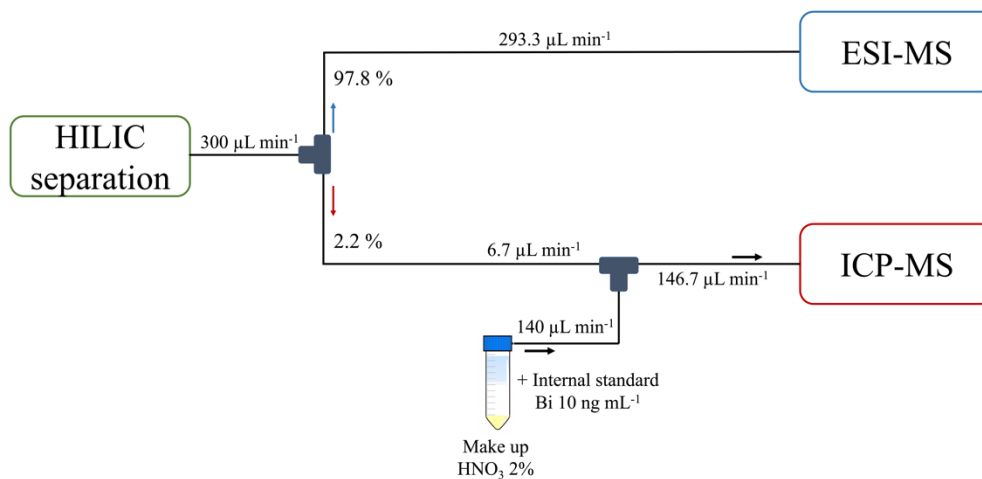
435

436



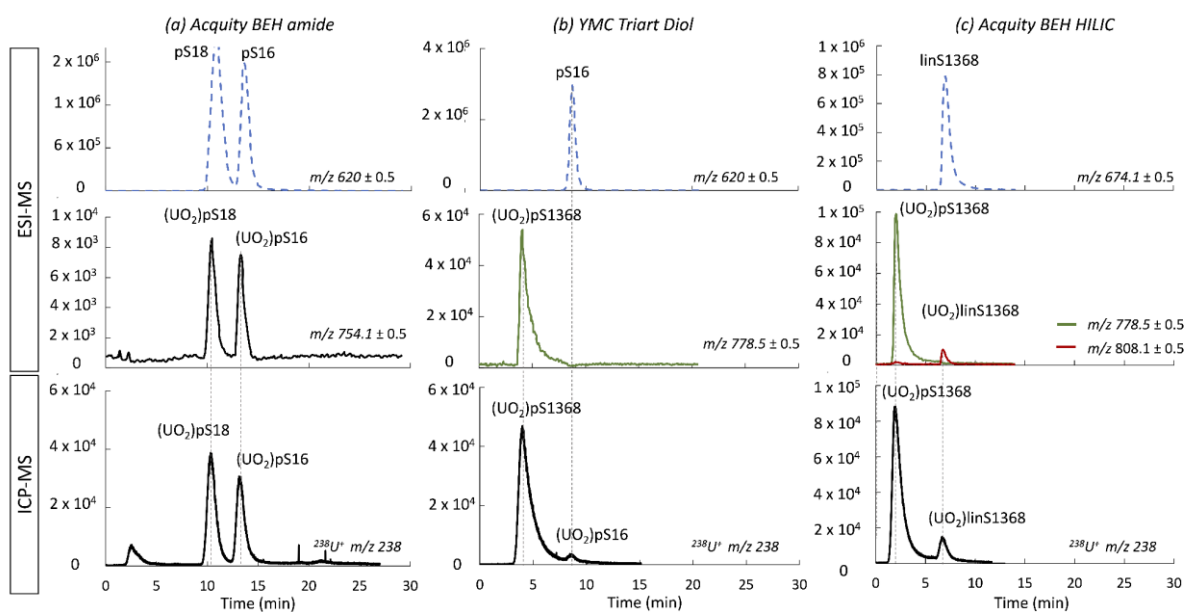
438
 439 Fig.1: Multi-phosphorylated peptides considered in this work. Peptides were named according to their cyclic/linear structure
 440 and to the number and position of the pSer residues. Di-phosphorylated peptides pS18 and pS16, contain two pSer residues in
 441 trans 1,6 and cis 1,8 positions respectively. Tetra-phosphorylated pS1368 and linS1368 peptides contain four pSer residues in
 442 1,3,6 and 8 position but have cyclic and linear structure.

443



444
 445 Fig.2: Schematic representation of the simultaneous coupling of HILIC to ESI-MS and ICP-MS according to [11].

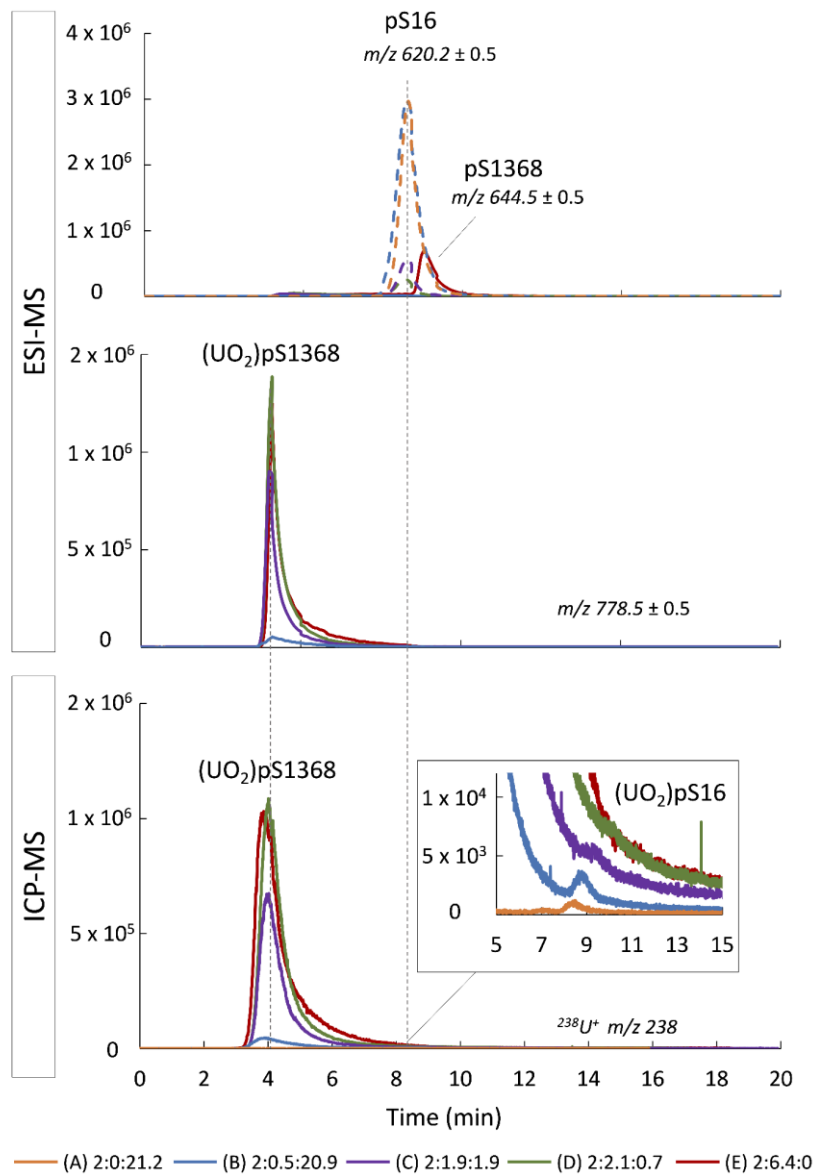
446



447

448 Fig.3: Chromatograms simultaneously acquired by ESI-MS using SIM mode for targeted monitoring of m/z ratios of free
 449 peptides and UO_2 (peptide) complexes and by ICP-MS recording the ^{238}U signal with an integration time of 90 ms. (a)
 450 Sample: 2UO_2^{2+} :10pS16:10pS18. Column: Acquity BEH amide 100 x 2.1 mm; 1.7 μm . Mobile phase: 70/30 ACN/ H_2O v/v
 451 with 20 mmol L^{-1} $\text{NH}_4\text{CH}_3\text{CO}_2$. (b) Sample: 2UO_2^{2+} :0.5pS1368:20pS16. Column: YMC Triart Diol 100 x 2,1 mm; 1,9 μm .
 452 Mobile phase: 72/28 ACN/ H_2O v/v with 20 mmol L^{-1} $\text{NH}_4\text{CH}_3\text{CO}_2$. (c) Sample: 2UO_2^{2+} :0.5pS1368:3.5linS1368. Column:
 453 Acquity BEH HILIC 100 x 2,1; 1,7 μm . Mobile phase: 68/32 ACN/ H_2O v/v with 20 mmol L^{-1} $\text{NH}_4\text{CH}_3\text{CO}_2$. In all cases, the
 454 flow rate was 300 $\mu\text{L min}^{-1}$, the elution mode isocratic and $V_{\text{inj}} = 3 \mu\text{L}$.

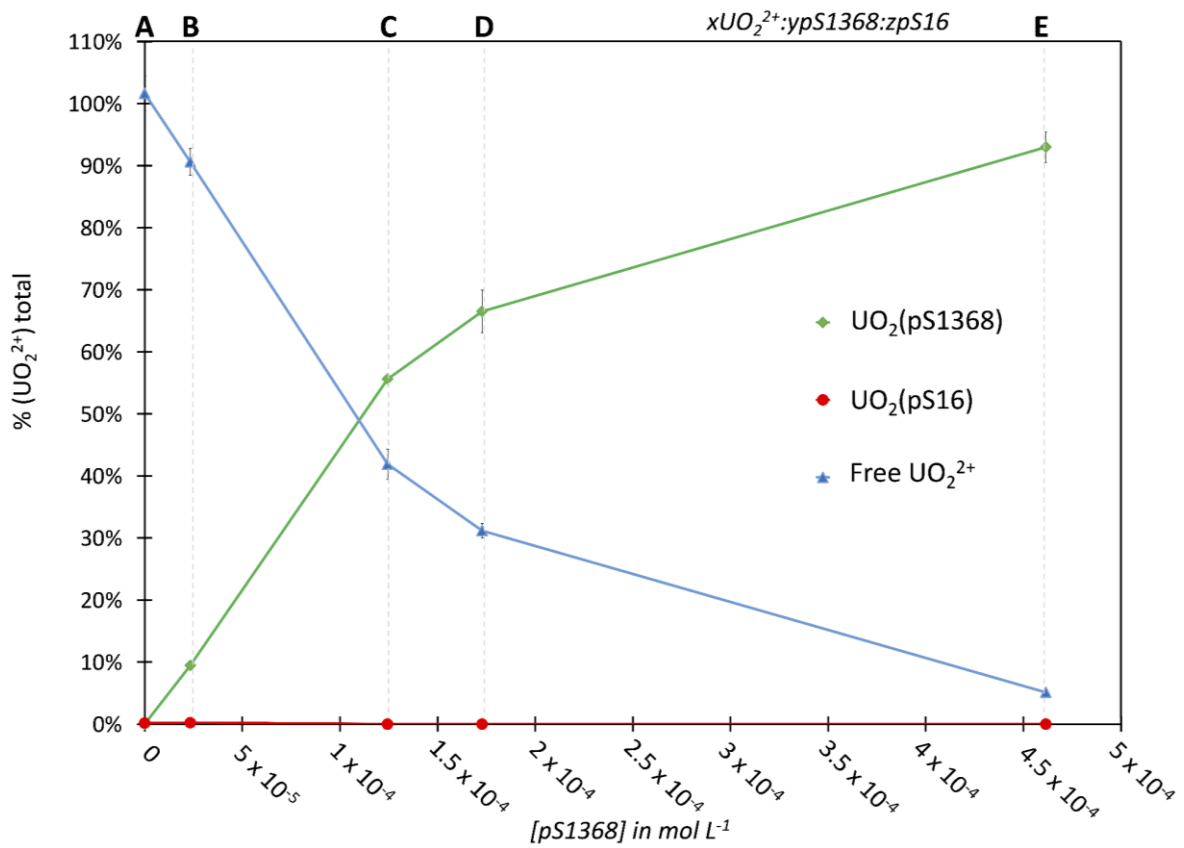
455



457

458 Fig.4: Chromatograms simultaneously acquired by ESI-MS using SIM mode for targeted monitoring of m/z ratios of free
 459 peptides and $\text{UO}_2(\text{peptide})$ complexes and by ICP-MS recording the ^{238}U signal with an integration time of 90 ms. Column:
 460 YMC Triart Diol 100 x 2.1 mm; 1.9 μm . Mobile phase: 72/28 ACN/ H_2O v/v with 20 mmol L^{-1} $\text{NH}_4\text{CH}_3\text{CO}_2$. Flow rate was
 461 300 $\mu\text{L min}^{-1}$, the elution mode isocratic and $V_{\text{inj}} = 3 \mu\text{L}$.

462



464

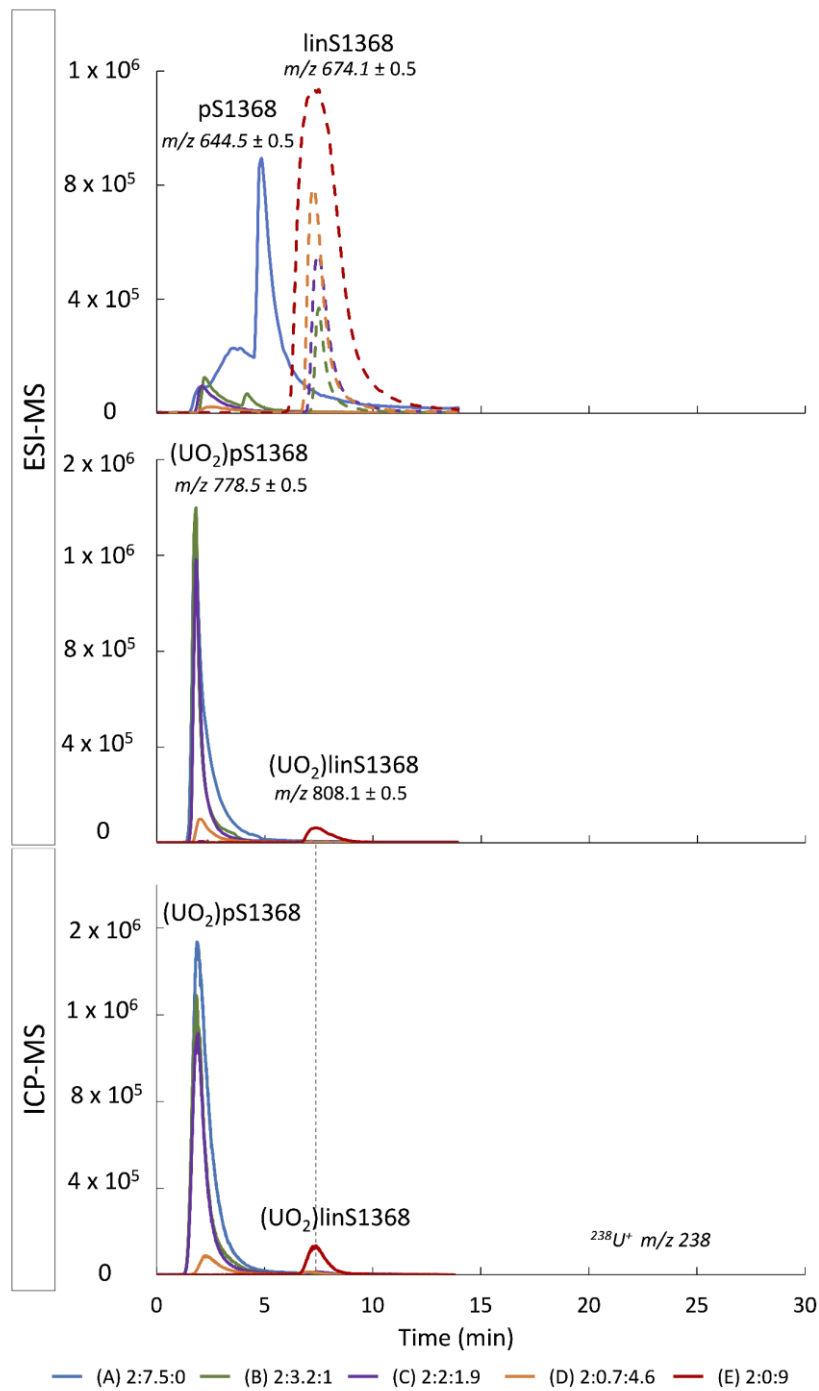
465 Fig.5 : Quantitative distribution of total UO_2^{2+} expressed in percentage (%) among the different complexes as a function of

466 pS1368 concentration and $x\text{UO}_2^{2+}:\text{ypS1368}:\text{zpS16}$ proportions in the samples (A) 2:0:21.2, (B) 2:0.5:20.9, (C) 2:1.9:1.9, (D)

467 2:2.1:0.7 and (E) 2:6.4:0 with average mass balance of $101.8 \pm 3\%$, $100.3 \pm 2\%$, $97.5 \pm 2\%$, $97.7 \pm 5\%$, $98.1 \pm 3\%$, respectively. The

468 dots correspond to the average of the values of two replicates and the error bars represent their standard deviation.

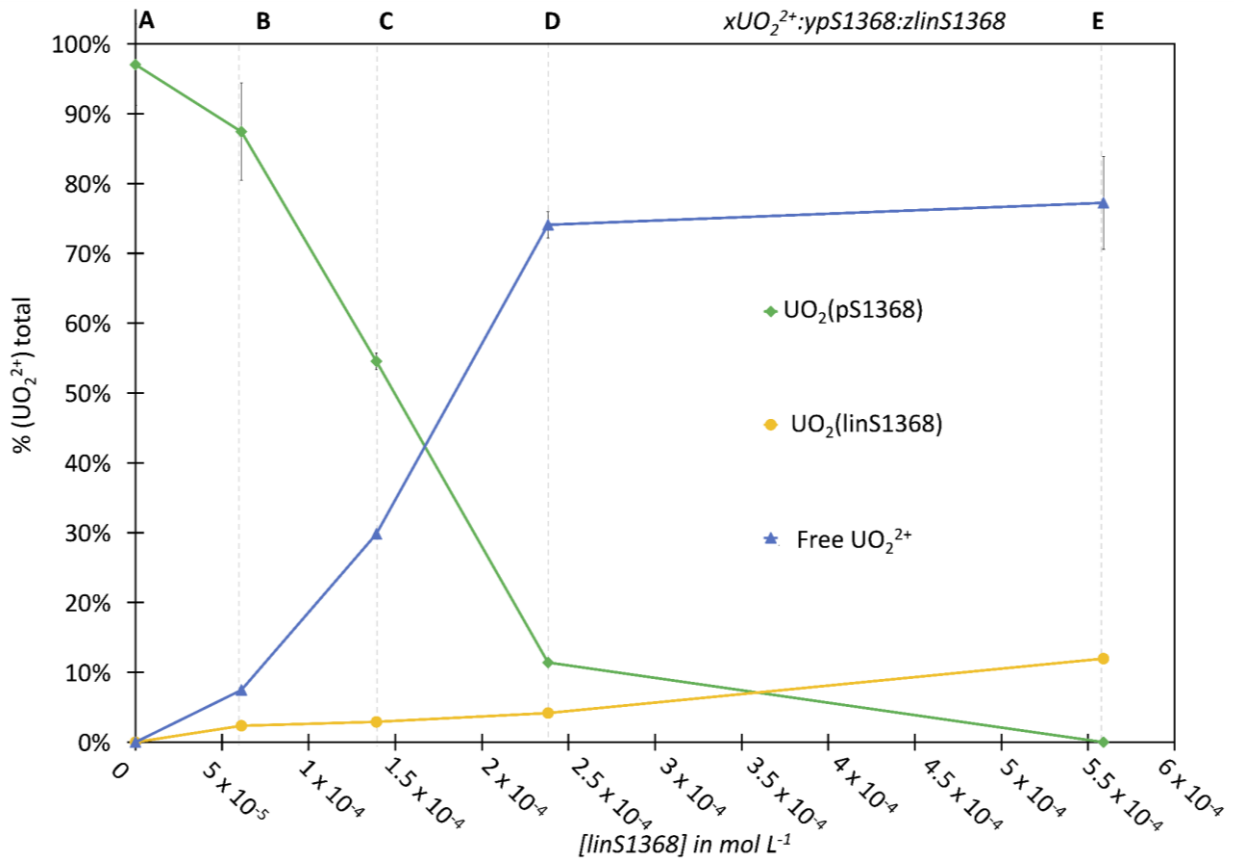
469



471

472 Fig.6: Chromatograms simultaneously acquired by ESI-MS using SIM mode for targeted monitoring of m/z ratios of free
 473 peptides and UO_2 complexes and by ICP-MS recording the ^{238}U signal with an integration time of 90 ms. Column: Acquity
 474 BEH HILIC 100 x 2,1 mm; 1,7 μm . Mobile phase: 68/32 ACN/ H_2O v/v with 20 mmol L^{-1} $NH_4CH_3CO_2$. Flow rate was 300
 475 $\mu L min^{-1}$, the elution mode isocratic and $V_{inj} = 3 \mu L$.

476



478

479 Fig.7 : Quantitative distribution of total UO_2^{2+} expressed in percentage (%) among the different complexes as a function of
 480 linS1368 concentration and the $x\text{UO}_2^{2+}:\text{ypS1368}:\text{zlinS1368}$ proportions in the samples (A) 2-7,5-0, (B) 2-3,2-1, (C) 2-2-1,9,
 481 (D) 2-0,7-4,6 and (E) 2-0-9 with average mass balance of $97.0 \pm 6\%$, $97.3 \pm 7\%$, $87.3 \pm 1\%$, $89.7 \pm 1\%$ and $89.2 \pm 6\%$, respectively.

482 The dots correspond to the average of the values of two replicates and the error bars represent their standard deviation.

483

484

485

486

487 **Figure captions**

488 Fig.1: Multi-phosphorylated peptides considered in this work. Peptides were named according to their
489 cyclic/linear structure and to the number and position of the pSer residues. Di-phosphorylated peptides
490 pS18 and pS16, contain two pSer residues in trans 1,6 and cis 1,8 positions respectively. Tetra-
491 phosphorylated pS1368 and linS1368 peptides contain four pSer residues in 1,3,6 and 8 position but
492 have cyclic and linear structure.

493
494 Fig.2: Schematic representation of the simultaneous coupling of HILIC to ESI-MS and ICP-MS
495 according to [11].

496
497 Fig.3: Chromatograms simultaneously acquired by ESI-MS using SIM mode for targeted monitoring of
498 m/z ratios of free peptides and $\text{UO}_2(\text{peptide})$ complexes and by ICP-MS recording the ^{238}U signal with
499 an integration time of 90 ms. (a) Sample: $2\text{UO}_2^{2+}:10\text{pS16}:10\text{pS18}$. Column: Acquity BEH amide 100 x
500 2.1 mm; 1.7 μm . Mobile phase: 70/30 ACN/ H_2O v/v with 20 mmol L^{-1} $\text{NH}_4\text{CH}_3\text{CO}_2$. (b) Sample:
501 $2\text{UO}_2^{2+}:0.5\text{pS1368}:20\text{pS16}$. Column: YMC Triart Diol 100 x 2,1 mm; 1,9 μm . Mobile phase: 72/28
502 ACN/ H_2O v/v with 20 mmol L^{-1} $\text{NH}_4\text{CH}_3\text{CO}_2$. (c) Sample: $2\text{UO}_2^{2+}:0.5\text{pS1368}:3.5\text{linS1368}$. Column:
503 Acquity BEH HILIC 100 x 2,1; 1,7 μm . Mobile phase: 68/32 ACN/ H_2O v/v with 20 mmol L^{-1}
504 $\text{NH}_4\text{CH}_3\text{CO}_2$. In all cases, the flow rate was 300 $\mu\text{L min}^{-1}$, the elution mode isocratic and $V_{\text{inj}} = 3 \mu\text{L}$.

505
506 Fig.4: Chromatograms simultaneously acquired by ESI-MS using SIM mode for targeted monitoring
507 of m/z ratios of free peptides and $\text{UO}_2(\text{peptide})$ complexes and by ICP-MS recording the ^{238}U signal with
508 an integration time of 90 ms. Column: YMC Triart Diol 100 x 2.1 mm; 1.9 μm . Mobile phase: 72/28
509 ACN/ H_2O v/v with 20 mmol L^{-1} $\text{NH}_4\text{CH}_3\text{CO}_2$. Flow rate was 300 $\mu\text{L min}^{-1}$, the elution mode isocratic
510 and $V_{\text{inj}} = 3 \mu\text{L}$.

511
512 Fig.5 : Quantitative distribution of total UO_2^{2+} expressed in percentage (%) among the different
513 complexes as a function of pS1368 concentration and $x\text{UO}_2^{2+}:y\text{pS1368}:z\text{pS16}$ proportions in the
514 samples (A) 2:0:21.2, (B) 2:0.5:20.9, (C) 2:1.9:1.9, (D) 2:2.1:0.7 and (E) 2:6.4:0 with average mass

515 balance of $101.8\pm 3\%$, $100.3\pm 2\%$, $97.5\pm 2\%$, $97.7\pm 5\%$, $98.1\pm 3\%$, respectively. The dots correspond to
516 the average of the values of two replicates and the error bars represent their standard deviation.

517
518 Fig.6: Chromatograms simultaneously acquired by ESI-MS using SIM mode for targeted monitoring of
519 m/z ratios of free peptides and UO_2 complexes and by ICP-MS recording the ^{238}U signal with an
520 integration time of 90 ms. Column: Acquity BEH HILIC 100 x 2,1 mm; 1,7 μm . Mobile phase: 68/32
521 ACN/ H_2O v/v with 20 mmol L^{-1} $\text{NH}_4\text{CH}_3\text{CO}_2$. Flow rate was 300 $\mu\text{L min}^{-1}$, the elution mode isocratic
522 and $V_{\text{inj}} = 3 \mu\text{L}$.

523
524 Fig.7 : Quantitative distribution of total UO_2^{2+} expressed in percentage (%) among the different
525 complexes as a function of linS1368 concentration and the $x\text{UO}_2^{2+}:\text{ypS1368}:\text{zlinS1368}$ proportions in
526 the samples (A) 2-7,5-0, (B) 2-3,2-1, (C) 2-2-1,9, (D) 2-0,7-4,6 and (E) 2-0-9 with average mass balance
527 of $97.0\pm 6\%$, $97.3\pm 7\%$, $87.3\pm 1\%$, $89.7\pm 1\%$ and $89.2\pm 6\%$, respectively. The dots correspond to the
528 average of the values of two replicates and the error bars represent their standard deviation.

References

- [1] M. Ma, R. Wang, L. Xu, M. Xu, S. Liu, Emerging health risks and underlying toxicological mechanisms of uranium contamination: Lessons from the past two decades, *Environment International*. 145 (2020) 106107. <https://doi.org/10.1016/j.envint.2020.106107>.
- [2] E. Ansoborlo, O. Prat, P. Moisy, C. Den Auwer, P. Guilbaud, M. Carriere, B. Gouget, J. Duffield, D. Doizi, T. Vercouter, C. Moulin, V. Moulin, Actinide speciation in relation to biological processes, *Biochimie*. 88 (2006) 1605–1618. <https://doi.org/10.1016/j.biochi.2006.06.011>.
- [3] C. Basset, O. Averseng, P.-J. Ferron, N. Richaud, A. Hagège, O. Pible, C. Vidaud, Revision of the Biodistribution of Uranyl in Serum: Is Fetuin-A the Major Protein Target?, *Chem. Res. Toxicol.* 26 (2013) 645–653. <https://doi.org/10.1021/tx400048u>.
- [4] L. Qi, C. Basset, O. Averseng, E. Quéméneur, A. Hagège, C. Vidaud, Characterization of UO_2^{2+} binding to osteopontin, a highly phosphorylated protein: insights into potential mechanisms of uranyl accumulation in bones, *Metallomics*. 6 (2014) 166–176. <https://doi.org/10.1039/C3MT00269A>.
- [5] A. Garai, P. Delangle, Recent advances in uranyl binding in proteins thanks to biomimetic peptides, *Journal of Inorganic Biochemistry*. 203 (2020) 110936. <https://doi.org/10.1016/j.jinorgbio.2019.110936>.
- [6] F.A. Laporte, C. Lebrun, C. Vidaud, P. Delangle, Phosphate-Rich Biomimetic Peptides Shed Light on High-Affinity Hyperphosphorylated Uranyl Binding Sites in Phosphoproteins, *Chemistry – A European Journal*. (2019). <https://doi.org/10.1002/chem.201900646>.
- [7] C. Lebrun, M. Starck, V. Gathu, Y. Chenavier, P. Delangle, Engineering Short Peptide Sequences for Uranyl Binding, *Chem. Eur. J.* 20 (2014) 16566–16573. <https://doi.org/10.1002/chem.201404546>.
- [8] M. Starck, N. Sisommay, F.A. Laporte, S. Oros, C. Lebrun, P. Delangle, Preorganized Peptide Scaffolds as Mimics of Phosphorylated Proteins Binding Sites with a High Affinity for Uranyl, *Inorg. Chem.* 54 (2015) 11557–11562. <https://doi.org/10.1021/acs.inorgchem.5b02249>.
- [9] M. Starck, F.A. Laporte, S. Oros, N. Sisommay, V. Gathu, P.L. Solari, G. Creff, J. Roques, C. Den Auwer, C. Lebrun, P. Delangle, Cyclic Phosphopeptides to Rationalize the Role of Phosphoamino Acids in Uranyl Binding to Biological Targets, *Chem. Eur. J.* 23 (2017) 5281–5290. <https://doi.org/10.1002/chem.201605481>.
- [10] F. Laporte, Y. Chenavier, A. Botz, C. Gateau, C. Lebrun, S. Hostachy, C. Vidaud, P. Delangle, A Simple Fluorescence Affinity Assay to Decipher Uranyl-Binding to Native Proteins, *Angew Chem Int Ed.* 61 (2022). <https://doi.org/10.1002/anie.202203198>.
- [11] E. Blanchard, A. Nonell, F. Chartier, A. Rincel, C. Bresson, Evaluation of superficially and fully porous particles for HILIC separation of lanthanide–polyaminocarboxylic species and simultaneous coupling to ESIMS and ICPMS, *RSC Adv.* 8 (2018) 24760–24772. <https://doi.org/10.1039/C8RA02961J>.
- [12] H. Peng, B. Hu, Q. Liu, Z. Yang, X. Lu, R. Huang, X.-F. Li, M.J. Zuidhof, X.C. Le, Liquid chromatography combined with atomic and molecular mass spectrometry for speciation of arsenic in chicken liver, *Journal of Chromatography A*. 1370 (2014) 40–49. <https://doi.org/10.1016/j.chroma.2014.10.012>.
- [13] A. Hagège, T.N.S. Huynh, M. Hébrant, Separative techniques for metalloproteomics require balance between separation and perturbation, *TrAC Trends in Analytical Chemistry*. 64 (2015) 64–74.

<https://doi.org/10.1016/j.trac.2014.08.013>.

- [14] J. Köster, R. Shi, N. von Wirén, G. Weber, Evaluation of different column types for the hydrophilic interaction chromatographic separation of iron-citrate and copper-histidine species from plants, *Journal of Chromatography A*. 1218 (2011) 4934–4943. <https://doi.org/10.1016/j.chroma.2011.03.036>.
- [15] E. Paredes, E. Avazeri, V. Malard, C. Vidaud, P.E. Reiller, R. Ortega, A. Nonell, H. Isnard, F. Chartier, C. Bresson, Evidence of isotopic fractionation of natural uranium in cultured human cells, *Proc Natl Acad Sci USA*. 113 (2016) 14007–14012. <https://doi.org/10.1073/pnas.1610885113>.
- [16] A. Leclercq, A. Nonell, J.L. Todolí Torró, C. Bresson, L. Vio, T. Vercouter, F. Chartier, Introduction of organic/hydro-organic matrices in inductively coupled plasma optical emission spectrometry and mass spectrometry: A tutorial review. Part I. Theoretical considerations, *Analytica Chimica Acta*. 885 (2015) 33–56. <https://doi.org/10.1016/j.aca.2015.03.049>.
- [17] A. Leclercq, A. Nonell, J.L. Todolí Torró, C. Bresson, L. Vio, T. Vercouter, F. Chartier, Introduction of organic/hydro-organic matrices in inductively coupled plasma optical emission spectrometry and mass spectrometry: A tutorial review. Part II. Practical considerations, *Analytica Chimica Acta*. 885 (2015) 57–91. <https://doi.org/10.1016/j.aca.2015.04.039>.
- [18] M. Sutton, S.R. Burastero, Uranium(VI) Solubility and Speciation in Simulated Elemental Human Biological Fluids, *Chem. Res. Toxicol.* 17 (2004) 1468–1480. <https://doi.org/10.1021/tx049878k>.
- [19] A. Younes, G. Creff, M.R. Beccia, P. Moisy, J. Roques, J. Aupiais, C. Hennig, P.L. Solari, C. Den Auwer, C. Vidaud, Is hydroxypyridonate 3,4,3-LI(1,2-HOPO) a good competitor of fetuin for uranyl metabolism?, *Metallomics*. 11 (2019) 496–507. <https://doi.org/10.1039/C8MT00272J>.
- [20] C. Vidaud, M. Robert, E. Paredes, R. Ortega, E. Avazeri, L. Jing, J.-M. Guignonis, C. Bresson, V. Malard, Deciphering the uranium target proteins in human dopaminergic SH-SY5Y cells, *Arch Toxicol.* 93 (2019) 2141–2154. <https://doi.org/10.1007/s00204-019-02497-4>.
- [21] Y. Eb-Levadoux, S. Frelon, O. Simon, C. Arnaudguilhem, R. Lobinski, S. Mounicou, In vivo identification of potential uranium protein targets in zebrafish ovaries after chronic waterborne exposure, *Metallomics*. 9 (2017) 525–534. <https://doi.org/10.1039/C6MT00291A>.
- [22] S. Frelon, O. Simon, Y. Eb-Levadoux, S. Mounicou, Screening of potential uranium protein targets in fish ovaries after chronic waterborne exposure: Differences and similarities between roach and zebrafish, *Journal of Environmental Radioactivity*. 222 (2020) 106365. <https://doi.org/10.1016/j.jenvrad.2020.106365>.
- [23] Ł. Szyrwił, V. Liauchuk, L. Chavatte, R. Lobinski, In vitro induction and proteomics characterisation of a uranyl–protein interaction network in bovine serum, *Metallomics*. 7 (2015) 1604–1611. <https://doi.org/10.1039/C5MT00207A>.
- [24] A. Dedieu, F. Bérenguer, C. Basset, O. Prat, E. Quéméneur, O. Pible, C. Vidaud, Identification of uranyl binding proteins from human kidney-2 cell extracts by immobilized uranyl affinity chromatography and mass spectrometry, *Journal of Chromatography A*. 1216 (2009) 5365–5376. <https://doi.org/10.1016/j.chroma.2009.05.023>.
- [25] L. Abou Zeid, A. Pell, T. Tytus, P. Delangle, C. Bresson, Separation of multiphosphorylated cyclopeptides and their positional isomers by hydrophilic interaction liquid chromatography (HILIC) coupled to electrospray ionization mass spectrometry (ESI-MS), *Journal of Chromatography B*. 1177 (2021) 122792. <https://doi.org/10.1016/j.jchromb.2021.122792>.

- [26] M. Birka, K.S. Wentker, E. Lasmöller, B. Arheilger, C.A. Wehe, M. Sperling, R. Stadler, U. Karst, Diagnosis of Nephrogenic Systemic Fibrosis by means of Elemental Bioimaging and Speciation Analysis, *Anal. Chem.* 87 (2015) 3321–3328. <https://doi.org/10.1021/ac504488k>.
- [27] G. Weber, N. von Wirén, H. Hayen, Hydrophilic interaction chromatography of small metal species in plants using sulfobetaine- and phosphorylcholine-type zwitterionic stationary phases, *Journal of Separation Science*. 31 (2008) 1615–1622. <https://doi.org/10.1002/jssc.200800060>.
- [28] J. Vanhorn, H. Huang, Uranium(VI) bio-coordination chemistry from biochemical, solution and protein structural data, *Coordination Chemistry Reviews*. 250 (2006) 765–775. <https://doi.org/10.1016/j.ccr.2005.09.010>.
- [29] S. Safi, G. Creff, A. Jeanson, L. Qi, C. Basset, J. Roques, P.L. Solari, E. Simoni, C. Vidaud, C. Den Auwer, Osteopontin: A Uranium Phosphorylated Binding-Site Characterization, *Chemistry - A European Journal*. 19 (2013) 11261–11269. <https://doi.org/10.1002/chem.201300989>.
- [30] R. Pardoux, S. Sauge-Merle, D. Lemaire, P. Delangle, L. Guilloureau, J.-M. Adriano, C. Berthomieu, Modulating Uranium Binding Affinity in Engineered Calmodulin EF-Hand Peptides: Effect of Phosphorylation, *PLoS ONE*. 7 (2012) e41922. <https://doi.org/10.1371/journal.pone.0041922>.
- [31] S. Sauge-Merle, F. Brulfert, R. Pardoux, P.L. Solari, D. Lemaire, S. Safi, P. Guilbaud, E. Simoni, M.L. Merroun, C. Berthomieu, Structural Analysis of Uranyl Complexation by the EF-Hand Motif of Calmodulin: Effect of Phosphorylation, *Chem. Eur. J.* 23 (2017) 15505–15517. <https://doi.org/10.1002/chem.201703484>.
- [32] H. Zänker, K. Heine, S. Weiss, V. Brendler, R. Husar, G. Bernhard, K. Gloe, T. Henle, A. Barkleit, Strong Uranium(VI) Binding onto Bovine Milk Proteins, Selected Protein Sequences, and Model Peptides, *Inorganic Chemistry*. 58 (2019) 4173–4189. <https://doi.org/10.1021/acs.inorgchem.8b03231>.
- [33] F. Laporte, Compréhension des mécanismes de complexation de l'uranyle par les molécules du vivant: élaboration de peptides biomimétiques chélatants pour la détoxification, PhD Thesis, Grenoble Alpes, 2017.